Journal of Inorganic Biochemistry 200 (2019) 110800

Contents lists available at ScienceDirect

Journal of Inorganic Biochemistry

journal homepage: www.elsevier.com/locate/jinorgbio

In vitro tyrosinase, acetylcholinesterase, and HSA evaluation of dioxidovanadium (V) complexes: An experimental and theoretical approach

Otávio Augusto Chaves[a,b], Márcia Cristina Campos de Oliveira[b], Cristiane Martins Cardoso de Salles[c], Francisco Mainardi Martins[d], Bernardo Almeida Iglesias[e,*], Davi Fernando Back[d,*]

[a] Instituto SENAI de Inovação em Química Verde, Rua Morais e Silva N° 53, Maracanã, 20271030 Rio de Janeiro, RJ, Brazil
[b] Instituto de Química, Departamento de Química Orgânica, Universidade Federal Rural do Rio de Janeiro – UFRRJ, 23970-000 Seropédica, RJ, Brazil
[c] Instituto de Química, Departamento de Bioquímica, Universidade Federal Rural do Rio de Janeiro – UFRRJ, 23970-000 Seropédica, RJ, Brazil
[d] Laboratório de Materiais Inorgânicos, Departamento de Química, Universidade Federal de Santa Maria - UFSM, 97115-900 Santa Maria, RS, Brazil
[e] Laboratório de Bioinorgânica e Materiais Porfirínicos, Departamento de Química, Universidade Federal de Santa Maria – UFSM, 97105-900 Santa Maria, RS, Brazil

ARTICLE INFO

Keywords:
cis-Dioxidovanadium(V) complexes
Human serum albumin
Tyrosinase activity
Acetylcholinesterase activity

ABSTRACT

The present study reports the biological evaluation of vanadium(V) complexes (**1–3**) against three different proteins: tyrosinase, acetylcholinesterase (AChE), and human serum albumin (HSA), which were studied by spectroscopic techniques and molecular docking. Despite the synthesis and characterization of complexes **1** and **2** having already previously described, complex **3** is a novel dioxidovanadium(V) derivative. Complex **1** can activate both tyrosinase and AChE enzymes in about 11.5 and 47.0%, respectively. On the other hand, complexes **2** and **3** inhibited the same enzymes (1.30 and 46.0% for tyrosinase and 20.0 and 21.9% for AChE, respectively). Molecular docking calculations suggested that the presence of the hydroxyl group in complex **1** is essential to activate tyrosinase enzymes. According to theoretical analysis, hydrogen bonding, van der Waals, and hydrophobic forces are the main binding interactions for each V(V) complex and AChE. Moreover, the interaction between HSA and vanadium(V) complexes occurs *via* ground-state association, being only enthalpically driven for complexes **1** and **2** and entropically and enthalpically driven for complex **3**. The interaction is spontaneous for all samples and the binding modes do not perturb significantly the secondary and surface structures of the albumin. As there are few reported cases in the literature that explore vanadium complexes against these three proteins, the present results may contribute to future studies by offering different scaffolds to design new vanadium(V) complexes in the hyperpigmentation process and Alzheimer's disease.

1. Introduction

The field of metallopharmaceuticals has become an important field of medicinal chemistry due to therapeutic uses of metal-based drugs. Thus, in addition to vanadium being a relevant species in several biological processes, many of its complexes with organic derivatives have been proposed for treating several types of diseases, including diabetes, cancer, anti-parasitic, antiviral, anti-bacterial, phosphatase inhibitor, and cardioprotection [1–4]. Additionally, the speciation of vanadium complexes in blood serum has also been investigated mainly because of its direct impact on the pharmacokinetical profile of potential drugs, although much remains to be done concerning *in situ* real-time investigations [5]. Despite vanadium complexes presenting positive biological activity, they have yet to be used in the clinic phase and further research on vanadium-based drugs is still necessary not only in pharmacodynamic profiles, but also in the pharmacokinetical point of view.

Melanogenesis is a complex process with different stages that involve melanin synthesis and transport and melanosome release. Melanin is composed of pheomelanin and eumelanin and is synthesized in the melanocyte melanosomes. Melanin synthesis is mainly regulated by the enzyme tyrosinase, thus, an abnormal synthesis of melanin can be related to disorders in the tyrosinase activity, leading to skin conditions such as vitiligo, melasma, chloasma freckles, and inflammatory pigmentation [6,7]. Tyrosinase is a copper-containing polyphenol oxidative enzyme that plays a vital role in melanogenesis by catalyzing the hydroxylation of L-tyrosine to L-3,4-dihydroxyphenylalanine (L-DOPA), followed by L-DOPA oxidation to L-Dopaquinone, although tyrosinase may lead to various dermatological disorders including

* Corresponding author.
E-mail address: bernardopgq@gmail.com (B.A. Iglesias).

https://doi.org/10.1016/j.jinorgbio.2019.110800
Received 14 April 2019; Received in revised form 7 August 2019; Accepted 11 August 2019
Available online 29 August 2019
0162-0134/

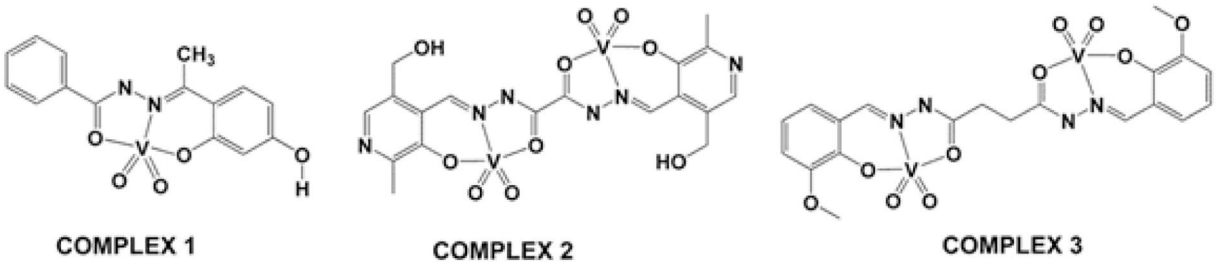

Fig. 1. Chemical representation for each dioxydovanadium(V) ion complexes – complexes **1–3**. It was chosen to evidence the complex ions of dioxydovanadium(V) without the respective counterions. Both complexes **1** and **3** are triethylammonium molecules and in the case of complex **2**, protonated DBU molecules are presented.

hyperpigmentation or hypopigmentation [8,9]. Recently, some hydrazide and vanadium(V) hydrazide complexes were evaluated against tyrosinase activity. The results showed that vanadium complexes had better activity than hydrazides without the presence of metal ions and variable degrees of inhibition potential [10]. Nevertheless, the development of tyrosinase inhibitors or activators for use as skin agents is still under evaluation.

Acetylcholinesterase (AChE) is a very important enzyme used to control transmission between neurons, which is when the process is either mediated or modulated by the neurotransmitter acetylcholine (ACh). Acetylcholine is released by the axon terminal or varicosities of the transmitter neuron into the extracellular space to interact with the receptors of the other neuron [11]. Some reversible AChE inhibitors have medical applications and are particularly important in treating Alzheimer's disease. When people develop Alzheimer's disease, their neurons degenerate, which leads to low neurotransmitter production, a process that induces serious memory problems [12]. Mild AChE inhibition has shown to have therapeutic relevance in treating Alzheimer's disease. In contrast, strong AChE inhibition may lead to cholinergic poisoning. In order to restore acetylcholine levels to normal (removing the offending AChE inhibitor), novel series of organic/inorganic AChE reactivators have been developed [13]. Recently, the possible effects of vanadium therapy on the kinetic parameters of brain membrane-bound and soluble AChE forms in alloxan-induced diabetic rats were reported and showed that sodium orthovanadate administration reversed diabetic conditions by decreasing blood glucose levels and normalizing blood hemoglobin A1C (Hb_{A1C}) levels. The same sodium orthovanadate may also normalize the levels of brain AChE, glutathione-S-transferase, and thiobarbituric acid reactive substances compared to diabetic state and control. Therefore, vanadate administration may protect against the direct action of lipid peroxidation on brain AChE and, in this way, possibly help prevent cholinergic neural dysfunction, which is one of the most common complications in diabetes [14].

Serum albumin is the most abundant plasma protein in the bloodstream. Human serum albumin (HSA) is a highly soluble negatively charged protein that helps maintain oncotic pressure of the human circulatory system and distribute different organic/inorganic compounds by interacting with several endogenous (*e.g.*, bilirubin and fatty acids) and exogenous (*e.g.*, drugs and xenobiotics) species [15]. Thus, HSA commonly plays a crucial role in the pharmacokinetic process of commercial and potential drugs, as whatever the therapeutic use envisaged for any compound, its pharmacokinetics must be addressed, namely how it is transported in the bloodstream [16]. From a structural point of view, HSA is a non-glycosylated polypeptide (585 amino acid residues and molecular weight 66,500 Da) that presents a heart-shaped structure containing three homologous domains (I, II, and III) divided into a pair of subdomains termed subdomain-A and subdomain-B. There is just one tryptophan residue (Trp-214) in the albumin structure and it is explored to investigate the albumin binding ability through spectroscopic techniques [17,18].

To have a physiological role, the metal ion or vanadium complex must first be transported and up-taken by cells. This process is most likely conducted by plasma proteins such as human serum transferrin (hTF), HSA, and immunoglobulin G (IgG) [19]. The interaction of V(IV) compounds, including bis(maltolato)oxovanadium(IV) (BMOV) and $[VO(dmpp)_2]$ complexes, with apotransferrin (apo-Tf), human serum albumin (HSA), and small bioligands present in blood serum has been studied by electron paramagnetic resonance (EPR) and circular dichroism (CD) [20–22]. In the case of HSA, mixed species *cis*-[VO(carrier)$_2$-(HSA)] complex involving hydrogen bonding and/or hydrophobic interactions with the protein surface have been proposed [23].

Considering the biological importance of vanadium-based drugs in the metallopharmaceutical field and the lack research on vanadium(V) derivatives against hyperpigmentation/hypopigmentation processes and Alzheimer's disease, the main goal of the present study is the biological evaluation of three vanadium complexes (complexes **1–3**) against tyrosinase and AChE activity. Additionally, a preliminary evaluation of the pharmacokinetic profile of complexes **1–3** was also performed using HSA as a model. All experimental data (spectroscopic approach) were correlated with theoretical analysis by molecular docking calculations. Complexes **1** and **2** have already been reported in the literature [4], however, complex **3** is a novel dimeric derivative (Fig. 1).

2. Material and methods

2.1. General

Commercially available tyrosinase from mushroom lyophilized enzyme, (*S*)-2-amino-3-(3,4-dihydroxyphenyl)-propanoic acid (L-DOPA), 2,2′,2″,2‴-(ethane-1,2-diylbis(azanetriyl))-tetraacetic acid (EDTA), dimethyl sulfoxide (DMSO - spectroscopic grade), HSA, AChE, acetylthiocholine iodide, 5,5′-Dithiobis-(2-nitrobenzamide) (DTNB), disodium hydrogen phosphate/sodium phosphate monobasic buffer (Na_2HPO_4/NaH_2PO_4, pH 7.5), phosphate buffered saline (PBS, pH 7.4), *o*-vanillin, succinic dihydrazide, and oxyvanadium(IV) acetylacetonate were purchased from Sigma-Aldrich Chemical Company. Acetonitrile (spectroscopic grade) was obtained from Tedia Ltd. One tablet of commercial PBS dissolved in 200 mL of Milli-Q water yields 1.00×10^{-2} M phosphate buffer, 2.70×10^{-3} M potassium chloride and 1.37×10^{-1} M sodium chloride. The synthesis of the ligand **L3** and complex **3** are described in the supplementary material (Schemes S1–S2).

Elemental CHN% analyses were obtained using a Perkin-Elmer CHN % 2400 equipment. ^{1}H and ^{13}C NMR spectra were recorded on a Bruker DPX-400 spectrometer at 400 (^{1}H) and 100 Hz (^{13}C), respectively. DMSO-d_6 was used as the solvent and as the internal reference. The chemical shifts are expressed in δ (ppm). UV–vis spectra were recorded on a Shimadzu UV-2600 spectrometer in DMSO solution. Cyclic voltammograms were recorded with an AutoLab PGSTAT128N Eco Chemie system at room temperature under argon atmosphere, using dry DMSO as a solvent. Electrochemical grade tetrabutylammoniumhexafluorophosphate ($TBAPF_6$) was used as supporting electrolyte.

Employing a standard three-component system we carried out the following experiments: a glassy carbon working electrode; a platinum wire auxiliary electrode and a platinum wire *pseudo*-reference electrode. Ferrocene was used as internal standard [24].

2.2. X-Ray crystallography

Data were collected on a Bruker D8 Venture Photon 100 diffractometer equipped with an Incoatec IμS high brilliance Mo-Kα X-ray tube with two-dimensional Montel micro-focusing optics. The structure was solved by direct methods using SHELXS [25]. Subsequent Fourier-difference map analyses yielded the positions of the non-hydrogen atoms. Refinements were carried out with the SHELXL package [25]. All refinements were made by full-matrix least-squares on F2 with anisotropic displacement parameters for all non–hydrogen atoms. Hydrogen atoms were included in the refinement in calculated positions but the atoms (of hydrogens) that are commenting performing special bond were located in the Fourier map. Drawings were done using DIAMOND for Windows [26]. Crystal data and structure refinement for the ligand **L3**, complex **3** and ORTEP representation of **L3** are described in the supplementary material (Tables S1–S4 and Fig. S2).

2.3. Tau parameter

A penta-coordinate complex can have its geometry and degree of distortion defined by calculating the parameter *tau* (τ), which considers the largest angles α and β in Eq. (1). The τ values vary between 0 and 1.0. If τ is between 0 and 0.5, the geometry is distorted quadratic pyramidal and, if it is between 0.5 and 1.0, the geometry is distorted trigonal bipyramid. The integer values 0 and 1.0 indicate the corresponding ideal geometries without distortion:

$$\tau = \frac{(\beta - \alpha)}{60} \quad (1)$$

By considering the penta-coordination, the connection angles, and τ parameter equal to 0.22, it is concluded that the metallic center has a distorted quadratic pyramidal geometry [4,27].

2.4. Spectroscopic analysis of the interaction HSA:complex 1–3

The interaction studies between HSA and vanadium(V) complexes (complexes **1**–**3**) were carried out through spectroscopic techniques. UV–vis and steady-state fluorescence spectra were measured on a Jasco J-815 fluorimeter to which a thermostated cuvette holder Jasco PFD-425S15F (0.1 °C accuracy) was coupled. All spectra were recorded with appropriate background corrections. The UV–vis spectrum for each vanadium complex (1.32×10^{-5} M) was measured in the 200–500 nm range, in PBS solution at 310 K. For steady-state fluorescence measurements (290–450 nm range and λ_{exc} = 280 nm, at 296 K, 303 K and 310 K), successive aliquots from a stock solution of each vanadium complex (1.00×10^{-3} M, in acetonitrile) were added to 3.0 mL of HSA solution (1.00×10^{-5} M, in PBS), leading to a final ligand concentration of 0.17; 0.33; 0.50; 0.66; 0.83; 0.99; 1.15 and 1.32×10^{-5} M. The steady-state fluorescence data were analyzed at the maximum fluorescence emission wavelength (λ_{exc} = 340 nm).

Since each vanadium complex showed significant absorption at the excitation and emission wavelengths (280 and 340 nm, respectively – Fig. S1 in the supplementary material), the inner filter correction was applied to the steady-state fluorescence data, according to Eq. (2) [28]:

$$F_{cor} = F_{obs} 10^{[(A_{ex}+A_{em})/2]} \quad (2)$$

where F_{cor} and F_{obs} are the corrected and observed fluorescence intensity values. A_{exc} and A_{em} are the absorbance values for the ligand at excitation (λ = 280 nm: ε = 33,859; 43,664; 50,329 $M^{-1} cm^{-1}$ in PBS for complexes **1**, **2**, and **3**, respectively) and emission wavelength (λ = 340: ε = 24,960; 29,501 and 22,550 $M^{-1} cm^{-1}$, in PBS for complexes **1**, **2**, and **3**, respectively).

Time-resolved fluorescence measurements were performed on Edinburgh Instruments fluorimeter model FL920 CD, equipped with an EPL laser (λ_{exc} = 280 ± 10 nm, λ_{em} = 340 nm; pulse width = 850 ps and energy per pulse = 1.8 μW). Fluorescence decays of 1.00×10^{-5} M HSA (3.0 mL in PBS) were measured in the absence and presence of each vanadium complex (1.32×10^{-5} M) at room temperature (*ca* 296 K). Time-resolved fluorescence decays were analyzed using the deconvolution software presents in the Edinburgh Instrument.

Circular dichroism (CD) spectra were measured in a spectropolarimeter Jasco J-815 employing a thermostatic cuvette holder Jasco PFD-425S15F with 0.1 °C accuracy. All spectra were recorded with appropriate background corrections. The CD spectra were recorded in the 200–260 nm range for HSA solution (1.00×10^{-6} M) without and in the presence of the maximum vanadium complex concentration used in the steady-state fluorescence measurements (1.32×10^{-5} M) at 310 K. CD results were expressed in terms of mean residue ellipticity (MRE) in deg. cm^2 $dmol^{-1}$, according to Eq. (3):

$$MRE = \frac{\theta}{(10.\ n.\ l.\ C_P)} \quad (3)$$

where θ, n, l, and C_p are the observed ellipticity (mdeg), number of amino acid residues (585 to HSA) [28], length of the optical cuvette (1.0 cm), and molar concentration of HSA (1.00×10^{-6} M), respectively.

Synchronous fluorescence (SF) spectra were recorded in a spectrofluorimeter model Xe900 from Edinburgh Instruments. The SF spectra were recorded for HSA (1.00×10^{-5} M) without and in the presence of each vanadium complex, at the same concentration range used in the steady-state fluorescence measurement. Spectra were recorded in the 240–320 nm range by setting Δλ = 15 nm (for tyrosine) and Δλ = 60 nm (for tryptophan) at room temperature (*ca.* 296 K).

2.5. Zeta potential analysis of the interaction HSA:complex 1–3

The surface charge of HSA in the absence and presence of each vanadium complex was characterized in terms of zeta potential (ZP) using a Brookhaven Instruments NanoBrook ZetaPALS. All measurements were performed with 10 runs at 296 K and results are reported in terms of ZP ± SD. The ZP was measured for HSA solution (1.00×10^{-5} M in PBS solution, pH 7.4) without and in the presence of complexes **1**, **2** or **3** at the maximum concentration used in the steady-state fluorescence measurements (1.32×10^{-5} M).

2.6. Tyrosinase assays

The UV–vis absorption spectra for tyrosinase assays were recorded on Shimadzu UV–vis spectrophotometer UV Mini 1240 (Kyoto, Japan), at room temperature (*ca* 296 K). Tyrosinase inhibition activity was measured by the method of Amorim and co-workers [29]. Each vanadium complex was mixed with L-DOPA (0.17 mM), EDTA (0.022 mM) and tyrosinase (50–100 units), in PBS solution (pH 7.4). Due to the fact that the vanadium(V) complexes showed different solubility in water, the concentration of the complexes **1**–**3** used to determine the inhibition percentage was 100, 66 and 133 μM, respectively. When the tyrosinase solution was added to the mixture, the absorbance was immediately measured at 475 nm and the formation of L-Dopaquinone was monitored for 30 min (Scheme 1).

The inhibition or activation percentage was calculated according to the Eq. (4) [29]:

$$\text{Inhibition or Activation}\% = \frac{[(B_{30} - B_0) - (A_{30} - A_0)]}{(B_{30} - B_0)} \times 100 \quad (4)$$

where B_0 and B_{30} are the absorbance of L-DOPA + tyrosinase at t = 0 min and t = 30 min, respectively. A_0 and A_{30} are the absorbance of L-DOPA + tyrosinase + inhibitor/activator at t = 0 min and

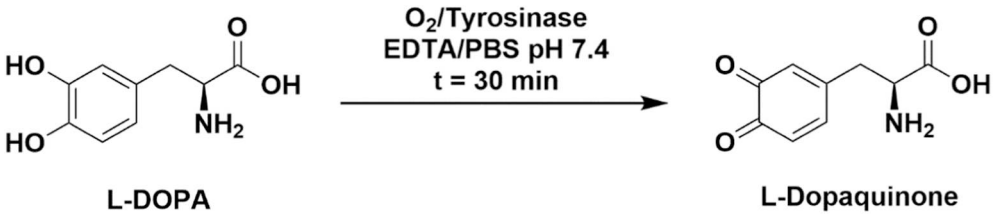

Scheme 1. Oxidation of L-DOPA to L-Dopaquinone by tyrosinase enzyme.

t = 30 min, respectively. In the Eq. (4), the possible interference of the absorbance of organic compounds was subtracted.

2.7. Acetylcholinesterase assays

Activity of AChE was determined using a Bio-Rad iMark microplate reader based on a modification of the Ellman method [30]. Compounds were dissolved in DMSO (maximum DMSO final concentration of 0.1%). The assay solution which contained 25 µL AChE, 10 µL acetylthiocholine iodide (1.5 mM), 85 µL Na_2HPO_4/NaH_2PO_4 buffer (pH 7.5; 0.1 M), and 22 µL tested compound solution (0.5 mM) were incubated at 298 K for 10 min. Then, 100 µL of DTNB (0.32 mM) were added and assay solution was incubated at 298 K for 10 min. The absorbance of each assay mixture was measured at 412 nm by UV–vis spectroscopy. In blanks solutions, tested compound solutions were not added.

2.8. Molecular docking analysis

The vanadium(V) derivatives structures **1–3** were obtained from X-ray crystallography data, recently published by Siqueira and collaborators [4]. The crystallographic structure of tyrosinase, AChE and HSA were obtained from the Protein Data Bank (PDB), with access code 2Y9X [31], 1ACJ [32] and 1N5U [28], respectively. Molecular docking was performed with GOLD 5.5 program (CCDC). Hydrogen atoms were added to the proteins according to the data inferred by the program on the ionization and tautomeric states. For tyrosinase, a 10 Å radius spherical cavity around the dicopper center was defined as the binding site for the molecular docking calculations. While, for AChE, a 10 Å radius spherical cavity around Phe-330 residue was defined as the binding site for the molecular docking calculations. Finally, for HSA a 10 Å radius spherical cavity around Trp-214 residue (in subdomain IIA) was defined and the molecular docking calculations for each vanadium complex were carried out. The scoring function used was "*GoldScore*", "*ChemPLP*", and "*ChemPLP*" for tyrosinase, AChE, and HSA, respectively [33]. The figures of the docking pose for the largest docking score value was generated with the PyMOL Delano Scientific LLC program.

3. Results and discussion

3.1. Synthesis of ligand *L3* and vanadium(V) complex *3*

Siqueira and co-workers [4] previously described synthetical procedures and full characterization of ligands/complexes **1** and **2**. Complex **3** was obtained by the reaction between **L3** and dioxyvanadium (V)-bis(acetylacetonate) complex $[VO_2(acac)_2]$ as starting material using methanol as a solvent and triethylamine (Et_3N) as a base. In this case, ligand **L3** and complex **3** were characterized by elemental analysis (CHN %), UV–vis, FTIR, nuclear magnetic resonance (^1H and ^{13}C for ligand **L3**), and cyclic voltammetry analysis. Experimental procedures and selected spectra of ligand **L3** and complex **3** are presented in the supplementary material (Schemes S1–S2 and Figs. S1–S6).

Elemental analyses of compounds **L3** and complex **3** are in accordance with the assigned chemical composition of the compounds. The ligand **L3** and complex **3** were characterized and confirmed by single-crystal X-ray diffraction analysis and Fourier Transformation Infrared spectroscopy (FTIR), showing characteristic stretches at ν(OH) 3450 cm^{-1}, ν(C=O) 1667 cm^{-1}, ν(C=N) 1576 cm^{-1}, and $\nu(C-O)_{phenol}$ in 1250 cm^{-1}. In the case of FTIR spectrum of the vanadium(V) complex **3**, characteristic stretches attributed to $\nu(N^+-H)$ were observed at 3425 cm^{-1}, ν(C=O) 1612 cm^{-1}, ν(C=N) 1563 cm^{-1}, $\nu(C-O)_{phenol}$ in 1252 cm^{-1}, $\nu(VO_2)_{asym}$ in 958 cm^{-1}, and $\nu(VO_2)_{sym}$ in 892 cm^{-1}, respectively [34–37].

The nuclear magnetic resonance (^1H and ^{13}C NMR) spectra and chemical shift attribution of ligand **L3** are shown in supplementary material (Figs. S5–S6). Hydrogen signals are assigned to iminic protons at the 11.68–11.28 ppm range, aromatic protons at the 8.35–6.83 ppm region, methoxyl groups at 3.80 ppm and aliphatic signals at the 2.93–2.55 ppm range. The ^{13}C NMR of ligand **L3** showed carbon signals at the high frequency range of the spectrum and chemical shifts at the 173.02–118.81 ppm range, while C13 signals of the electron donating group OCH_3 appeared at 55.85 ppm and aliphatic signals were observed at the 28.78–27.24 ppm region.

The absorption UV–vis spectrum of ligand **L3** was recorded in DMSO solution and revealed transition bands at 295 nm, which can be assigned to the intraligand $\pi \rightarrow \pi^*$ transition and 331 nm attributed to the $n \rightarrow \pi^*$ transition band (Fig. 2 and Table 1). The absorption electronic spectra of vanadium(V) complex **3** was conducted in DMSO and revealed transitions at 323 nm and 396 nm, respectively (Fig. 2 and Table 1). The transition bands of vanadium(V) compound is in accordance with dioxovanadium(V) derivatives in a distorted trigonal bipyramidal environment, which had their structures confirmed by X-ray diffraction analysis. No *d-d* type transitions were observed in the vanadium complex, revealing that the vanadium center is in the vanadium(V) oxidation state.

The electrochemical behavior of ligand **L3** and complex **3** were investigated by cyclic voltammetry (CV) experiments in a dry DMSO solution in the 1.0×10^{-4} M range by using 0.1 M of $TBAPF_6$ as a supporting electrode in an argon-saturated atmosphere at the −1.60 V to +1.20 V range *versus* a normal hydrogen electrode (NHE). For all compounds, the Fc/Fc^+ redox pair couple was used as the internal standard (see Materials and Methods). Cyclic voltammograms of ligand

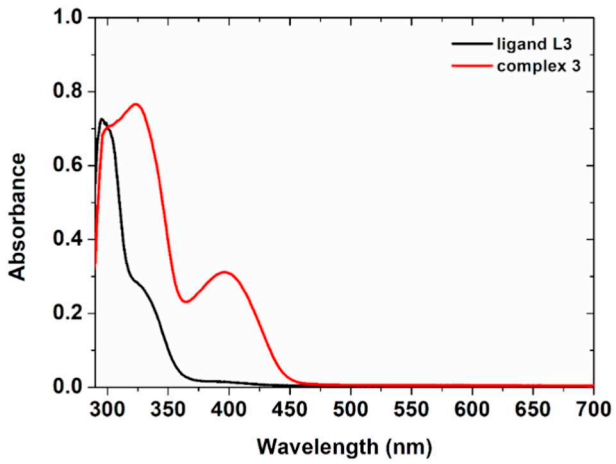

Fig. 2. Electronic UV–vis spectra for ligand **L3** and complex **3** in DMSO solutions ([**L3**] = [complex **3**] = 1.50×10^{-4} M).

Table 1
UV–vis transitions and redox potentials of ligand **L3** and complex **3**.

	UV–vis	Redox potential (*vs* NHE)		
Compound	λ, nm (ε; $M^{-1}\,cm^{-1}$)	E_{ox1}	E_{ox2}	E_{red1}
L3	295 (4833) and 331 (1720)	+0.326 V[a]	–	−1.186 V[b]
Complex **3**	323 (5113) and 396 (2080)	+0.430V[a]	+0.813V[a]	−0.924V[b]

[a] E_{pa} = anodic peak potential.
[b] E_{pc} = cathodic peak potential.

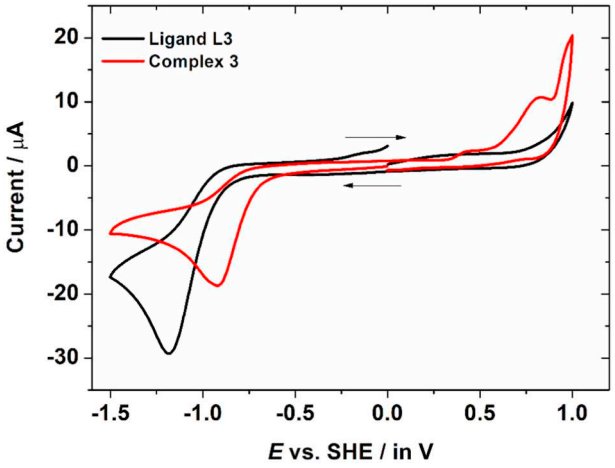

Fig. 3. Cyclic voltammograms of ligand **L3** and complex **3** solutions in dry DMSO, 0.1 M $TBAPF_6$, using glassy carbon electrode as work electrode, at scan rate 100 mV s^{-1}.

L3 presented a broad irreversible oxidation peak close to +0.326 V and irreversible reduction peak at −1.186 V, which may be attributed to ligand oxidation and reduction processes (Fig. 3 and Table 1).

For *cis*-dioxovanadium(V) complex **3** at the cathodic region, one redox peak was observed at −0.924 V, which is attributed to the reduction process V(V)/V(IV) center. At the positive range, two irreversible redox processes were observed. The oxidation peak at +0.430 V may be attributed to the ligand oxidation coordinated to the vanadium (V) center, following the next oxidation peak at +0.813 V, which can be assigned to the vanadium (V) complexes and vanadium (IV) species (Fig. 3 and Table 1) [4,38]. The formal potentials were calculated as the average of the cathodic (E_{pc}) and anodic (E_{pa}) peak potentials of this process.

3.2. Crystal structure of complex *3*

Crystal data collection and refinement of complex **3** are presented in the supplementary material (see Tables S3–S4). Complex **3** has two dioxovanadium centers coordinated at the two extremities of a molecule of the ONO chelating ligand by three distinct coordination sites: phenolate oxygen (O1), imine nitrogen (N1), and oxygen (O3) (Fig. 4) [39–41]. The adjacent nitrogen of the hydrazide function presents deprotonation, which generates a negative charge in the resonance between oxygen (O3) and nitrogen (N1). This causes the complex to present itself as an anionic species and be neutralized by the presence of a protonated triethylamine molecule (Et_3NH^+ - *triethylammonium ion*) [34,35,42,43]. The anionic character of the complex is likely responsible for its solubility in water.

The carbon-oxygen bond length of this function (C(9)-O(3)) is 1.293(6) Å, which is consistent with bonds for the enolate group [35,42,43]. The metal center is stabilized by double bonds with two oxygen atoms (O4 and O5), completing the coordination sphere and providing a coordination geometry of NO4 type.

Regarding the bond lengths, the values found are 1.898 (3) Å for V-O(1) (vanadium ion and phenolate group oxygen), 2.142 (3) Å for V-N (1) (vanadium ion and iminic nitrogen), 1.976(3) Å for VO(3) (vanadium ion and oxygen of enolate group), and 1.614(3)/1.647(3) Å for VO(4)/VO(5). All values are in agreement with data of *cis*-dioxovanadium(V) complexes already reported in the literature [4,35,42,43]. The presence of distortion in the coordination spheres by the connection angle values found in the metal centers are 150.74°(14) for O(3)-V-O (1), 99.86°(15) for O(3)-V-O(4), 137.27°(15) for N(1)-V-O(5), and 109.27°(18) for O(4)-V-O (5). The selected values for connecting length and angle for vanadium complex **3** are listed in the supplementary material (Table S4).

3.3. Binding parameters for the interaction HSA:complexes *1–3*

Human serum albumin (HSA) has strong intrinsic fluorescence at the 280-nm excitation wavelength mainly due to the presence of aromatic amino acid residues: tryptophan (Trp), tyrosine (Tyr), and phenylalanine (Phe). Tyrosine and phenylalanine residues have relatively low fluorescence quantum yield when compared to Trp residues. Thus, the dominant fluorescence at λ_{exc} = 280 nm is from Trp residue. This fluorescence emission is sensitive to the ligand presence and often used as a probe to identify the interaction of small ligands against serum albumin [44]. The steady-state fluorescence emission of HSA (1.00×10^{-5} M in PBS solution) with and without the presence of the maximum complex **1** concentration addition (1.32×10^{-5} M) at 310 K is shown in Fig. 5. The steady-state results for complexes **2** and **3** are presented as Fig. S7 in the supplementary material. Moreover, HSA exhibited strong fluorescence emission band at 340 nm. The fluorescence intensities of HSA reduced in the presence of each vanadium(V) complex and a weak red shift was also observed for complexes **1** and **2** (from 340 to 347 nm and 340 to 345 nm, respectively). This suggests that these ligands may be interacting with Trp-214 residue and the fluorescence chromophore of serum albumin is placed in a more hydrophilic environment upon ligand binding [45].

Generally, the binding interaction may be subdivided into a ground state or excited state complexation between fluorophore and quencher or structural change of protein around the fluorophore [46]. The main mechanism of HSA fluorescence quenching due to binding of quencher can be observed through steady-state and time-resolved fluorescence measurements. In general, Stern-Volmer analysis (Eq. (5A) and (5B) and *inset* in Fig. 4 for HSA:complex **1** and *inset* in the Figs. S7–S8 in the supplementary material) are useful to elucidate the mechanism involved in the quenching process [28]:

$$\text{(A)}\quad \frac{F_0}{F} = 1 + k_q\tau_0[Q] = 1 + K_{SV}[Q] \qquad \text{(B)}\quad k_q = \frac{K_{SV}}{\tau_0} \tag{5}$$

where F_0 and F are the steady-state fluorescence intensities of HSA in the absence and presence of each vanadium complex, respectively. Furthermore, K_{sv} and k_q are the Stern-Volmer quenching constant and bimolecular quenching rate constant, respectively, and [Q] and τ_o are the vanadium complex concentration and fluorescence lifetime of HSA without the quencher ($(5.61 \pm 0.22) \times 10^{-9}$ s).

Table 2 shows K_{SV} and k_q values for the interaction between HSA and each vanadium derivative at 296 K, 303 K and 310 K (*inset* of the Fig. 4).Since K_{SV} values decrease with the increasing of temperature and k_q values are larger than the diffusional collision quenching constant ($k_{diff} \approx 7.40 \times 10^9\ M^{-1}\,s^{-1}$, according to Smoluchowski-Stokes-Einstein theory at 298 K) [46] in all cases, indicates that the main fluorescence quenching mechanism is *via* static process. Thus, there is a ground state association between HSA and each compound [44].

Time-resolved fluorescence spectroscopy is an extension of steady-state fluorescence, which is a useful method to identify the main fluorescence quenching mechanism (static and/or dynamic). Fluorescence lifetimes (τ) occur as emissive decays from the singlet-state and can also be approximated as those decays occur in the time

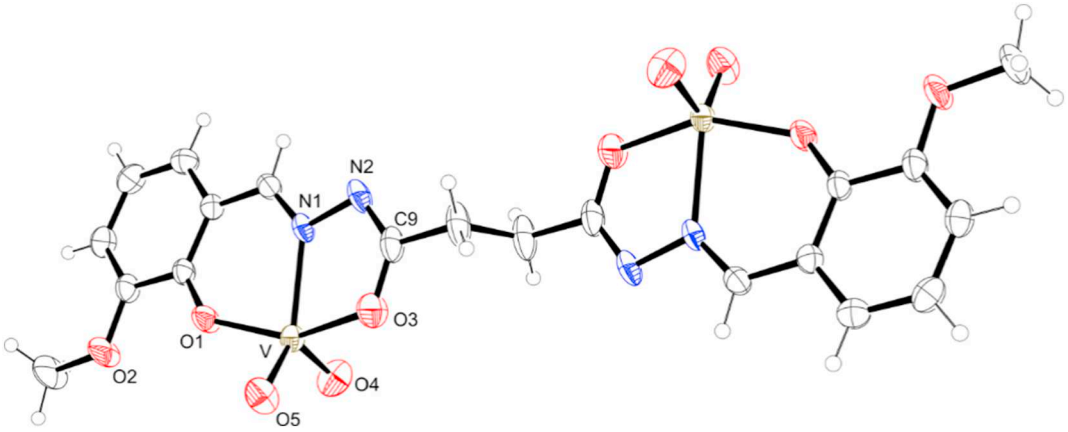

Fig. 4. Projection of the molecular structure of the complex **3** (complex ion). Thermal ellipsoids with 50% probability level. For better visualization, the triethylammonium ions were omitted.

region from picoseconds to nanoseconds. Nevertheless, HSA two fluorescence lifetimes (τ_1 = 1.48 ± 0.18 ns and τ_2 = 5.61 ± 0.22 ns), being the second one the most relative (82.0%). This data is in good accordance with the literature [47–51]. The presence of each vanadium derivative in the HSA solution decreases both fluorescence lifetimes, however, τ_1 and τ_2 with and without the presence of each complex are the same inside the standard deviation *e.g.* τ_1 = 1.45 ± 0.16 ns and τ_1 = 5.57 ± 0.20 ns, for HSA:complex **1**. Thus, static process is the main fluorescence quenching mechanism and in full agreement with the previously described K_{SV} and k_q values [52]. All fluorescence lifetime plots and values are presented in the supplementary material (Fig. S9 and Table S5).

Evaluating the binding constant between the serum albumin and a ligand is an important parameter to understand drug bioavailability. If binding affinity is low, the initial step of pharmacokinetics (drug absorption) is infeasible. In the case of moderate binding affinity of bioactive substances to serum albumin, drug absorption and distribution to various tissues are feasible. Finally, when binding affinity is high, drug absorption is feasible in spite of distribution to the required tissues being limited as a result of complex stability, which, in turn, adversely affects the pharmacokinetics of the drug [47,52]. The modified Stern-Volmer equation (Eq. (6)) can be used to obtain information on the binding constant between HSA and ligands:

$$\frac{F_0}{F_0 - F} = \frac{1}{fK_a[Q]} + \frac{1}{f} \quad (6)$$

where F_o and F are the steady-state fluorescence intensities of HSA in the absence and presence of each vanadium complex, K_a, f, and [Q] are the modified Stern-Volmer binding constant, and the fraction of the initial fluorescence that is accessible to the quencher ($f \approx 1.00$) and vanadium complex concentration, respectively. Fig. S9 in the supplementary material depicts the modified Stern-Volmer plots for the interaction HSA:complexes **1–3** and Table 2 shows K_a values at 296 K, 303 K, and 310 K. The K_a values for each vanadium complex decrease as temperatures increase, which also confirms the static fluorecence mechanism [53]. Additionally, the K_a values in the order of $10^5\,M^{-1}$ for HSA:complex **3** indicate strong binding ability of this vanadium complex and albumin protein pocket. On the other hand, K_a values in the range of 10^5–$10^4\,M^{-1}$ and 10^4–$10^3\,M^{-1}$ for complexes **1** and **2**, respectively, indicate moderate to weak interactions [54].

The thermodynamics of the interaction process yield a close insight to the mechanistic aspects involved. The interaction between drugs and biomacromolecules involve different types of bindings, such as electrostatics, hydrogen bondings, van der Waals interactions,

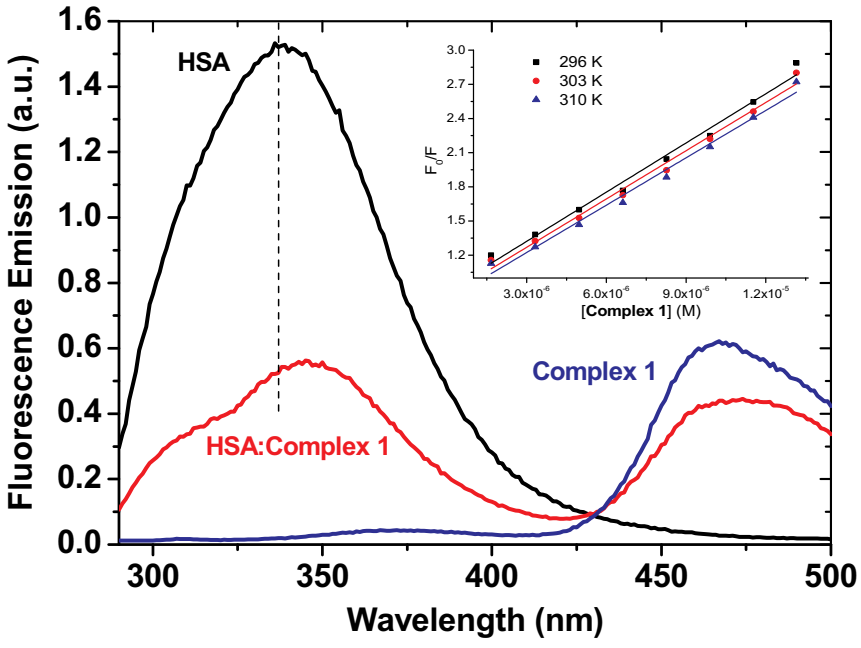

Fig. 5. Steady-state fluorescence emission spectra for HSA without and in the maximum addition of complex **1**, as well as complex **1** without the presence of albumin at pH 7.4 and 310 K. [HSA] = 1.00×10^{-5} M, [Complex **1**] = 1.32×10^{-5} M. *Inset*: Stern-Volmer plots for the interaction between HSA and complex **1** at 296 K, 303 K and 310 K.

Table 2
Binding parameters (K_{SV}, k_q, K_a, ΔH°, ΔS° and ΔG°) for the interaction HSA:complexes **1–3** at 296 K, 303 K and 310 K.

Complex	T (K)	K_{SV} ($\times 10^4$) (M^{-1})	k_q ($\times 10^{12}$) ($M^{-1}\,s^{-1}$)	K_a ($\times 10^4$) (M^{-1})	ΔH° (kJ mol^{-1})	ΔS° (kJ $mol^{-1}\,K^{-1}$)	ΔG° (kJ mol^{-1})
1	296	14.4 ± 0.1	25.7	11.2 ± 0.26			−28.7
	303	14.1 ± 0.1	25.2	6.32 ± 0.26	−68.1 ± 4.2	−0.133 ± 0.014	−27.8
	310	13.9 ± 0.1	24.7	3.21 ± 0.26			−26.9
2	296	1.07 ± 0.03	1.91	5.73 ± 0.26			−27.5
	303	1.05 ± 0.02	1.89	1.53 ± 0.26	−127 ± 8	−0.339 ± 0.026	−24.3
	310	0.88 ± 0.02	1.57	0.56 ± 0.03			−22.7
3	296	67.4 ± 0.4	120	26.3 ± 0.26			−30.7
	303	63.6 ± 0.3	113	23.0 ± 0.26	−12.8 ± 1.0	0.0606 ± 0.003	−31.2
	310	62.3 ± 0.2	111	20.8 ± 0.26			−31.6

Obs.: r^2 for K_{SV}, k_q: 0.9802–0.9985; r^2 for K_a: 0.9971–0.9999 and r^2 for ΔH°, ΔS° *and* ΔG°: 0.9887–0.9981.

hydrophobics, and steric contacts with the binding site [55]. The enthalpy (ΔH°) and entropy changes (ΔS°) can be obtained using Vant'Hoff equation (Eq. (7A)) and from these values Gibbs' free energy change (ΔG°) can be obtained by employing Eq. (7B) [47,52]:

$$\text{(A)}\quad \ln K_a = -\frac{\Delta H^0}{RT} + \frac{\Delta S^0}{R} \qquad \text{(B)}\quad \Delta G^0 = \Delta H^0 - T\Delta S^0 \tag{7}$$

where ΔH°, ΔS°, and ΔG° are the enthalpy, entropy, and Gibbs' free energy, respectively, R is the gas constant ($R = 8.314 \times 10^{-3}$ kJ $mol^{-1}\,K^{-1}$), T is the temperature (296 K, 303 K, and 310 K), and K_a the modified Stern-Volmer binding constant. Depending on the sign of thermodynamic parameters, the mode of interactions are categorized as [50–56]: (i) $\Delta H^\circ > 0$, $\Delta S^\circ > 0$ correspond to hydrophobic forces; (ii) $\Delta H^\circ < 0$, $\Delta S^\circ < 0$ correspond to van der Waals interaction and hydrogen-bond formation; (iii) $\Delta H^\circ < 0$, $\Delta S^\circ > 0$ correspond to electrostatic/ionic interaction.

Fig. S10 in the supplementary material depicts Vant'Hoff plot for the interaction HSA:complexes **1–3** and Table 2 shows the thermodynamic parameters (ΔH°, ΔS°, and ΔG°) for each sample. According to Ross and Subramanian's theory [56], for the interaction HSA:complex **1** and HSA:complex **2**, negative values for ΔH° and ΔS° are related to van der Waals interaction and/or hydrogen bonding. On the other hand, for the interaction HSA:complex **3**, the negative and positive value for ΔH° and ΔS°, respectively, suggest electrostatic interactions as the main binding force. Additionally, $\Delta S^\circ > 0$ can also be related to hydrophobic effects - desolvation of both protein cavity and complex **3** structure upon binding [57]. These results are different from those obtained for *cis*-[VO (carrier)$_2$-(HSA)] complex in the literature [23].

The negative values for ΔG° support the assertion that the binding process is spontaneous. According to Gibbs' free energy equation, negative and positive values for ΔH° and ΔS°, respectively, can contribute to the negative sign of ΔG°. Since complexes **1** and **2** showed $\Delta H^\circ < 0$ and $\Delta S^\circ < 0$, the binding process is only enthalpically driven. On the other hand, complex **3** showed $\Delta H^\circ < 0$ and $\Delta S^\circ > 0$, indicating that the binding process is entropically and enthalpically driven, which can contribute to higher K_a values [58].

3.4. Perturbation on the albumin structure upon compound binding

Circular dichroism (CD) spectroscopy is a useful technique to determine the possible influence of the interaction process on the secondary structure of the proteins. As shown in Fig. 6 for HSA:complex **1**, two negative absorption peaks in the UV range (208 and 222 nm) can be found in the CD spectra of HSA, which represent the α-helical structure through $\pi \rightarrow \pi^*$and $n \rightarrow \pi^*$transition, respectively [59]. All CD spectra are presented in the supplementary material – Fig. S11. The loss of α-helical content of the protein due to ligand binding was calculated as significant molar residual ellipticities (MRE) to free and combined HSA from MRE values at 208 and 222 nm using Eq. (8A) and (8B):

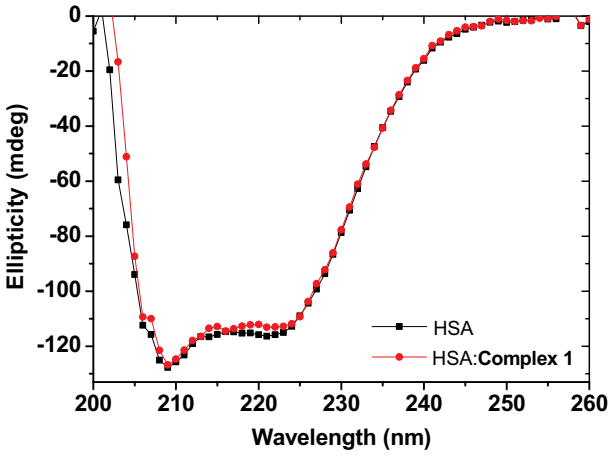

Fig. 6. CD spectra for HSA without and in the presence of complex **1** at pH 7.4 and 310 K. [HSA] = 1.00×10^{-6} M and [Complex **1**] = 1.32×10^{-5} M.

$$\text{(A)}\quad \alpha\text{-}helix\% = \left[\frac{(-MRE_{208} - 4000)}{(33000 - 4000)}\right] \times 100 \qquad \text{(B)}\quad \alpha\text{-}helix\% = \left[\frac{(-MRE_{222} - 2340)}{30300}\right] \times 100 \tag{8}$$

where MRE_{208} and MRE_{222} are the significant molar residual ellipticities (deg.cm^2.$dmol^{-1}$) at 208 and 222 nm, respectively. The quantitative CD results for HSA:complexes **1–3** are depicted in Table 3. The α-helix content of the secondary structure of HSA in the absence and presence of each vanadium complex barely changed, *e.g.* from 61.7 to 57.8% at 208 nm (variation of 3.90%) and from 58.1 to 56.0% at 222 nm (variation of 2.10%) for HSA:complex **1**. These quantitative calculations further confirm that the binding HSA:complexes **1–3** occurs with a relatively small change in the secondary structure of HSA [60].

Zeta potential (ZP - ζ) is a useful and feasible parameter to characterize the surface charge properties of proteins. Changes in the ZP of a protein may imply conformational changes in its structure, surface modifications, aggregation, and/or unfolding/denaturation processes.

Table 3
Quantitative α-helix % for the association HSA:complexes **1–3** at 208 and 222 nm (310*K*). [HSA] = 1.00×10^{-6} M and [Complexes **1–3**] = 1.32×10^{-5} M.

	Free HSA α-helix %		HSA:complexes 1–3	
Complex	208 nm	222 nm	208 nm	222 nm
1	61.7	58.1	57.8	56.0
2	61.9	58.4	59.7	56.9
3	62.5	58.9	60.7	55.9

Therefore, the ZP of a protein can be used as an indicator of protein stability upon ligand binding [61]. Table S6 in the supplementary material shows the ZP values for HSA with and without the presence of each vanadium complex. The ZP values of HSA changed after the addition of vanadium(V) complexes **1–3**, although the changes are in accordance with the standard error of the measurements, *e.g.* -9.06 ± 1.82 mV and −8.87 ± 1.50 mV for HSA and HSA:complex **1**, respectively. This suggests that there is no significant structural change on the protein surface with the addition of each vanadium derivative [55].

Synchronous fluorescence (SF) spectroscopy is a convenient and fast method to study changes in the microenvironments of tyrosine (Tyr) and tryptophan (Trp) residues of proteins when the differences between the emission and excitation wavelengths are 15 nm and 60 nm, respectively [58]. The effect of different concentrations of complexes **1–3** on Tyr and Trp residues of HSA is depicted in Figs. S12–S14 of the supplementary material.

There is no significant evidence of blue or red shift in the maximum emission of HSA upon successive ligand addition at $\Delta\lambda = 15$ nm in all samples, indicating that the microenvironment around tyrosine (Tyr) has no obvious changes [62]. On the other hand, there is a weak red shift upon successive addition of complex **1** (from 277 to 280 nm) and complex **2** (from 277 to 281 nm) at $\Delta\lambda = 60$ nm, indicating that the amino acid residues located near tryptophan Trp-214 are located in a more hydrophilic environment upon ligand binding.

3.5. Theoretical analysis of the albumin binding pocket

As previously described by Sudlow et al., there are two main binding sites in the HSA structure: Sudlow's site I and II, which are located in the subdomain IIA and IIIA, respectively. The first one presents high affinity for warfarin, while the second presents high affinity to ibuprofen [63]. According to the literature, Sudlow's site I, which is where tryptophan Trp-214 residue can be found, is the main binding site for some vanadium complexes, such as bis(maltolato)oxovanadium(IV), anionic $[V^{V}O_2(maltol)_2]^-$, $[V^{V}O_2(dmpp)(OH)(H_2O)]^-$, and $[V^{V}O_2(dmpp)_2]^-$ complexes [23]. In order to analyze the main intermolecular interactions between each studied compound and the amino acid residues present in the interaction cavity located in the subdomain IIA (Sudlow's site I), molecular docking calculations were carried out.

The best docking pose for the interaction between HSA:complexes **1–3** inside Sudlow's site I (subdomain IIA) are depicted in Fig. 7. Table S7 in the supplementary material shows the main amino acid residues and their corresponding intermolecular forces involved in the binding process for HSA:complexes **1–3**. Molecular docking results suggested hydrogen bonding and van der Waals forces as the main intermolecular interactions for each inorganic complex, however, hydrophobic interactions *via t*-Stacking was also detected for HSA:complex **2** and HSA:-complex **3**. For example, the oxygen from vanadium group of complex **1** interacts *via* hydrogen bonding with tryptophan Trp-214 residue within a distance of 2.80 Å. The oxygen atom from the phenol group of the ligand structure is a potential acceptor for hydrogen bonding with lysisne (Lys-198) residue within a distance of 3.50 Å. The hydrogen atom from the hydroxyl group of the amino acid residue Ser-453 is also a donor for hydrogen bonding with the nitrogen atom of the ligand structure within a distance of 3.00 Å. On the other hand, valine (Val-343); leucine (Leu-480); arginine (Arg-483) and proline (Pro-485) residues interact with complex **1** *via* van der Waals forces within a distance of 3.60, 2.30, 2.40, and 3.90 Å, respectively. Overall, molecular docking results are in good agreement with the intermolecular forces suggested by thermodynamic results.

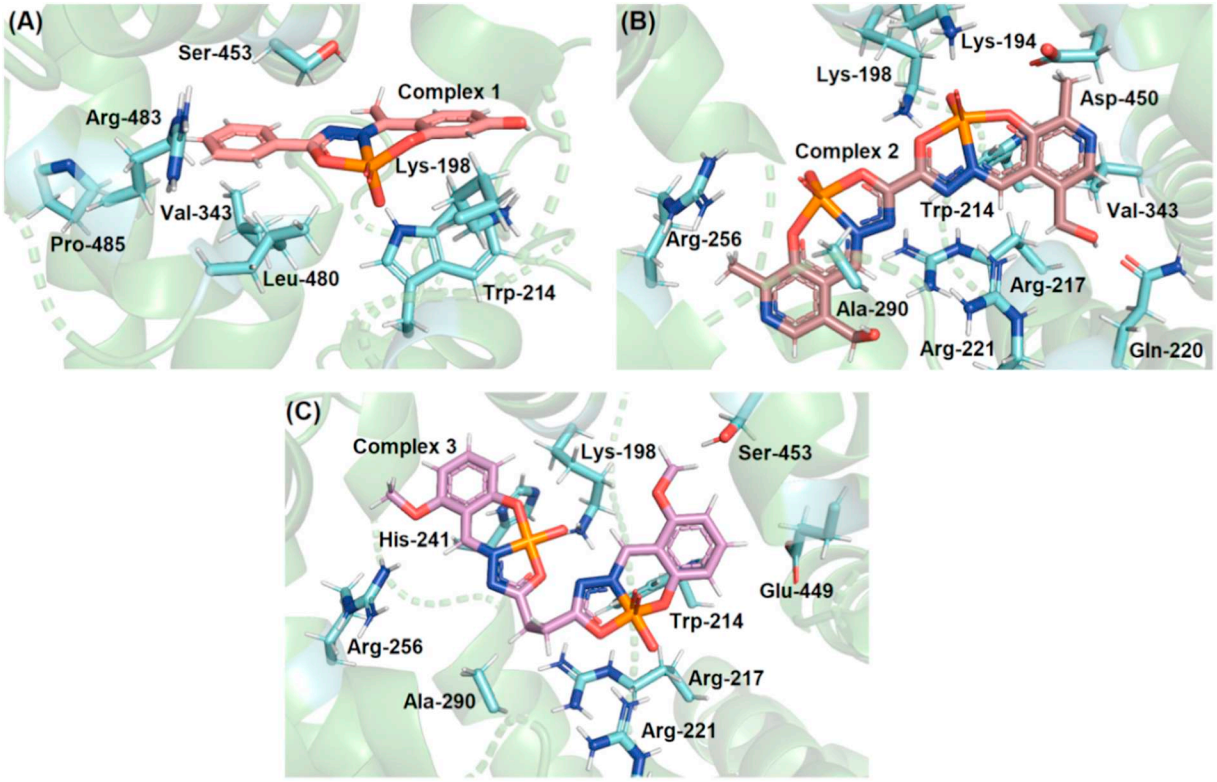

Fig. 7. Molecular docking results for the interaction between HSA:complex **1** (A), HSA:complex **2** (B) and HSA:complex **3** (C) in Sudlow's site I (*ChemPLP* function). Complexes **1–3** and selected amino acid residues are in beige, brown, magenta and cyan, respectively. Elements' colors: hydrogen, oxygen, nitrogen, and vanadium are represented in white, red, dark blue, and orange, respectively. (For interpretation of the references to colour in this figure legend, the reader is referred to the web version of this article.)

3.6. Tyrosinase and AChE evaluation – experimental and theoretical analysis

Complex **1** activated tyrosinase activity at about 11.5%, while complexes **2** and **3** inhibited tyrosinase activity at about 1.30 and 46.0%, respectively. By comparing the results of the complexes that can inhibit tyrosinase from others available in the literature (*e.g.* hydrazides) [10], it is plausible that that hydrize-based vanadium complexes are more active than vanadium complexes based on pyridoxals and resorcinols. Since complex **1** presented the ability to activate tyrosinase activity and the other vanadium complexes inhibited < 50% of tyrosinase activity, the IC_{50} value was not determined. In order to offer an atomic view of the activity of each *cis*-dioxovanadium(V) complex against tyrosinase, molecular docking calculations were carried out (Fig. 8A–C). Molecular docking results suggested that the hydroxyl group of complex **1** can interact with Cu(II) ions (cofactor essential to the tyrosinase activity) within a distance of 2.20 Å, being essential to the activation detected by experimental assays.

On the other hand, complexes **2** and **3** do not interact with Cu(II) ions through the hydroxyl group, but through the methyl group *via* van der Waals forces within a distance of 2.70 and 2.20 Å, respectively. Additionally, molecular docking also detected van der Waals and hydrophobic interactions as the main intermolecular forces for the interaction between each inorganic complex and amino acid residues in the tyrosinase active binding pocket, however, hydrogen bonding was also suggested for complexes **1** and **2**. The main amino-acid residues that participate in the interaction tyrosinase:complexes **1–3** are shown in Table S8 of the supplementary material. For example, the oxygen atom from the vanadium group of complex **1** is a potential acceptor for hydrogen bonding with the amide group of the aspargine (Asn-152) residue within a distance of 2.10 Å. The amino acid residues valine and phenylalanine Val-140, Phe-156, Val-172, and Phe-181 interact *via* hydrophobic forces with the aromatic rings of complex **1** within a distance of 2.70, 3.40, 3.70, and 2.40 Å, respectively. Finally, the interaction *via* van der Waals forces was also detected between three histidines (His-47, His-136, and His-151 residues) and complex **1** within a distance of 2.00, 2.20, and 2.30 Å, respectively.

The biological assays of vanadium(V) derivatives against the AChE enzyme presented similar ability when compared to tyrosinase (complex **1** can activate the enzyme, while complexes **2** and **3** can inhibit it). According to the experimental data, complex **1** is a potential activator in about 47.0% of AChE enzyme activity. On the other hand, complexes

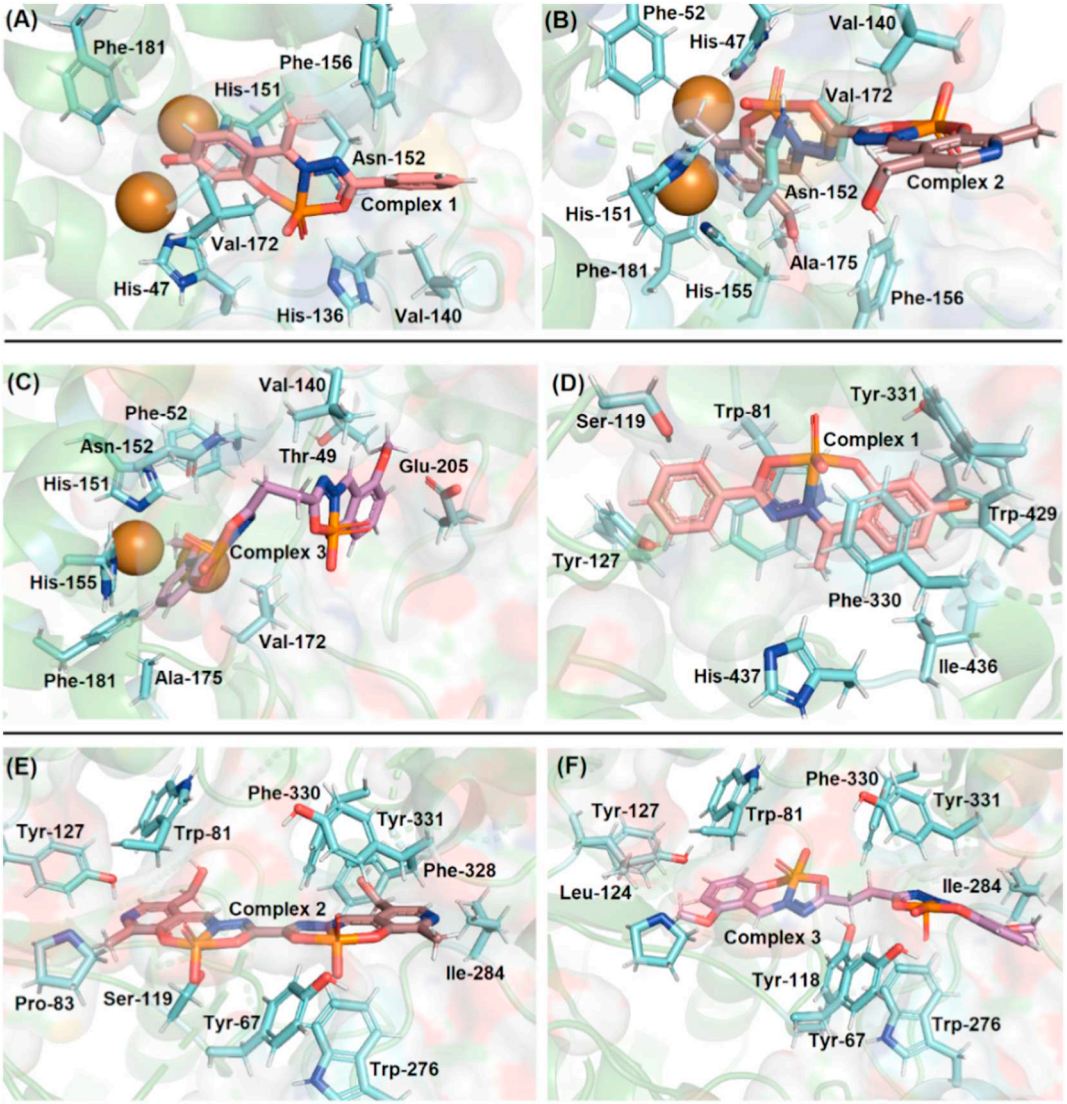

Fig. 8. Best docking poses for each inorganic complex toward tyrosinase (A, B and C), and AChE (D, E and F). Complexes **1–3** and selected amino acid residues are in beige, brown, magenta and cyan, respectively. Elements' colors: hydrogen, oxygen, nitrogen, and vanadium are represented in white, red, dark blue, and orange, respectively. Cu(II) ions are represented as spheres in sandy brown. (For interpretation of the references to colour in this figure legend, the reader is referred to the web version of this article.)

2 and **3** inhibited enzyme activity in about 20.0 and 21.9%, respectively. The half maximal inhibitory concentration (IC_{50}) value can be determined only for compounds that present inhibition ability, therefore, it cannot be determined in the case of AChE:complex **1**. Generally, compounds that present inhibition percentage 50% below the maximum concentration of inhibitor that does not precipitate in the medium, the IC_{50} value is difficult to be determined (complex **2** and **3** fits in this case).

In order to offer an atomic view of the activity of each vanadium complex for AChE, molecular docking calculations were also carried out (Fig. 8D–F). Molecular docking results suggested hydrogen bonding, van der Waals, and hydrophobic interactions as the main intermolecular forces. The main amino-acid residues that participate in the interaction AChE:complexes **1–3** are shown in Table S8 of the supplementary material. For example, the hydrogen from the phenol group of tyrosine Tyr-331 residue is a potential donor for hydrogen bonding with oxygen from the vanadium group of complex **1** within a distance of 2.80 Å. On the other hand, the aromatic ring of complex **1** can interact *via* van der Waals forces with serine Ser-119; tyrosine Tyr-127; tryptophan Trp-429 and histidine His-437 residues within a distance of 3.10, 2.80, 2.70, and 2.40 Å, respectively. Finally, amino acid residue tryptophan Trp-81 interacts *via* π-Stacking with the aromatic moiety of vanadium(V) complex **1** within a distance of 3.70 Å and phenylalanine Phe-330 and isoleucine Ile-436 residues interact *via* hydrophobic forces with vanadium(V) complex **1** structure within a distance of 2.60 and 2.10 Å, respectively.

Overall, the vanadium(V) complex **1** can activate both tyrosinase and AChE activity, and vanadium(V) complexes **2** and **3** can inhibit both enzymes. In the case of tyrosinase metalloenzyme, the interaction of each vanadium complex against Cu(II) ions is essential for the biological activity, thus, theoretical calculations suggested that the presence of the hydroxyl group in a vanadium complex can activate tyrosinase activity. In the case of AChE, complex **1** presented high ability to activate this enzyme activity, being a good scaffold for the design of potential AChE activators.

4. Conclusion

Ligand **L3** and vanadium(V) complex **3** were synthetized and fully characterized by spectroscopic and structural analysis. According to biological evaluation, vanadium(V) complex **1** can activate both tyrosinase and AChE activity (11.5 and 47.0%, respectively), and vanadium(V) complexes **2** and **3** can inhibit both enzymes (1.30 and 46.0% for tyrosinase and 20.0 and 21.9% respectively for AChE). In the case of tyrosinase metalloenzyme, the interaction of each vanadium complex against Cu(II) ions is essential for biological activity, thus, theoretical calculations suggest that the presence of the hydroxyl group in a vanadium complex can activate tyrosinase activity. In the case of AChE, complex **1** presented high ability to activate this enzyme, being a good scaffold to design potential AChE activators. Steady-state and time-resolved fluorescence analysis revealed that each vanadium complex is able to interact with HSA *via* ground-state association (k_q values higher than k_{diff} and fluorescence lifetime values are the same with and without the presence of complexes **1–3**). The K_a values in the order of $10^5\ M^{-1}$ for HSA:complex **3** indicate strong binding, while K_a values in the range of 10^5–$10^4\ M^{-1}$ and 10^4–$10^3\ M^{-1}$ for complexes **1** and **2**, respectively, indicate moderate to weak interaction. Zeta potential and CD results indicated that the interaction HSA:complexes **1–3** does not perturb significantly the secondary and surface structure of the albumin. Finally, molecular docking results suggested hydrogen bonding and van der Waals forces as the main intermolecular interaction for each inorganic complex inside subdomain IIA, however, hydrophobic interactions *via t*-Stacking was also detected for HSA:complexes **2–3**. Since in there are few cases reported in the literature that explore vanadium complexes against tyrosinase, AChE, and HSA, the studied vanadium(V) complexes presented good results to be used to design novel potential mettalodrugs, explored in the hyperpigmentation process and Alzheimer's disease.

Abbreviations

HSA	Human serum albumin
AChE	acetylcholinesterase enzyme
L-DOPA	(*S*)-2-amino-3-(3,4-dihydroxyphenyl)-propanoic acid
Hb_{A1C}	Hemoglobin A1C
BMOV	bis(maltolato)oxovanadium(IV)
apo-Tf	apotransferrin
EDTA	2,2′,2″,2‴-(ethane-1,2-diylbis(azanetriyl))-tetraacetic acid
DMSO	Dimethyl sulfoxide
FTIR	Fourier Transformation Infrared Spectroscopy
^{1}H NMR	Hydrogen nuclear magnetic resonance
^{13}C NMR	Carbon nuclear magnetic resonance
CV	cyclic voltammetry
DTNB	acetylthiocholine iodide; 5, 5′-Dithiobis-(2-nitrobenzamide)
PBS	phosphate buffer saline
CD	Circular dichroism
ZP	Zeta potential

Acknowledgements

This research was supported by the Brazilian funding agencies: Coordenação de Aperfeiçoamento de Pessoal de Nível Superior (CAPES), Conselho Nacional de Desenvolvimento Científico e Tecnológico (CNPq) and Fundação de Amparo à Pesquisa do Estado do Rio Grande do Sul (FAPERGS). D.F.B – acknowledges FAPERGS (Edital: Edital 02/2017 - Programa Pesquisador Gaúcho (PqG) – Process/Termo de Outorga N. 17/2551-0000963-0), PROEX/CAPES and CNPq (Universal-Process: 424515/2018-4 and PG-2016 (Process: 303011/2016-5)). B.A.I. –acknowledges CNPq (Universal-Process: 409150/2018-5 and PG-2016 (Process: 304711/2018-7)).

Appendix A. Supplementary data

CCDC (1936486 and 1910265) contain the supplementary crystallographic data for the ligand **L3** and the complex **3**, respectively. These data can be obtained free of charge *via* http://www.ccdc.cam.ac.uk/conts/retrieving.html, or from the Cambridge Crystallographic Data Centre, 12 Union Road, Cambridge CB2 1EZ, UK; fax: (+44) 1223–336–033; or e–mail: deposit@ccdc.cam.ac.uk. Supplementary data to this article can be found online at https://doi.org/10.1016/j.jinorgbio.2019.110800.

References

[1] M. Brownlee, Nature 414 (2001) 813–820.
[2] K.H. Thompson, K. Bohmerle, E. Polishcuk, C. Martins, P. Toleikis, J. Tse, V. Yuen, J.H. McNeil, C. Orvig, J. Inorg. Biochem. 98 (2004) 2063–2070.
[3] D.C. Han, M.-Y. Lee, K.D. Shin, S.B. Jeon, J.M. Kim, K.-H. Son, H.-C. Kim, H.-M. Kim, B.-M. Kwon, J. Biol. Chem. 279 (2004) 6911–6920.
[4] J.D. Siqueira, A.C.O. Menegatti, H. Terenzi, M.B. Pereira, D. Roman, E.F. Rosso, P.C. Piquini, B.A. Iglesias, D.F. Back, Polyhedron 130 (2017) 184–194.
[5] J.C. Pessoa, S. Etcheverry, D. Gambino, Coord. Chem. Rev. 301 (2015) 24–48.
[6] C.S. Kim, S.G. Noh, Y. Park, D. Kang, P. Chun, H.Y. Chung, H.J. Jung, H.R. Moon, Molecules 23 (2018) 2725–2738.
[7] H. Ando, H. Kondoh, M. Ichihashi, V.J. Hearing, J. Investig. Dermatol. 127 (2007) 751–761.
[8] H. Liu, Y. Zhu, T. Wang, J. Qi, X. Liu, Molecules 23 (2018) 2612–2623.
[9] S. Ito, K. Wakamatsu, Photochem. Photobiol. 84 (2008) 582–592.
[10] S. Sultan, U. Ashiq, R.A. Jamal, M. Mahroof-Tahir, R.S. Ahmad, Z. Shaikh, J. Chem. Soc. Pak. 40 (2018) 327–334.
[11] H. Tang, Y.-B. Wei, C. Zhang, F.X. Ning, W. Qiao, S.L. Huang, L. Ma, Z.S. Huang, L.Q. Gu, Eur. J. Med. Chem. 44 (2009) 2523–2532.
[12] E.C. Petronilho, M.N. Rennó, N.G. Castro, F.M.R. da Silva, A.C. Pinto, J.D. Figueroa-Villar, J. Enzyme Inhib. Med. Chem. 31 (2016) 1069–1078.
[13] S.F. McHardy, H.-Y.L. Wang, S.V. McCowen, M.C. Valdez, Expert Opin. Ther. Pat. 27 (2017) 455–476.
[14] D.A. Ghareeb, H.M. Hussen, Neurosci. Lett. 436 (2008) 44–47.

[15] M. Poór, S. Kunsági-Máté, M. Bálint, C. Hetényi, Z. Gerner, B. Lemli, J. Photochem. Photobiol. B 170 (2017) 16–24.
[16] T. Mukherjee, J.C. Pessoa, A. Kumar, A.R. Sarkar, Inorg. Chim. Acta 426 (2015) 150–159.
[17] S.N. Save, S. Choudhary, J. Mol. Liq. 265 (2018) 807–817.
[18] O.A. Chaves, B. Mathew, D. Cesarin-Sobrinho, B. Lakshminarayanan, M. Joy, G.E. Mathew, J. Suresh, J.C. Netto-Ferreira, J. Mol. Liq. 242 (2017) 1018–1026.
[19] J.C. Pessoa, G. Gonçalves, S. Roy, I. Correia, S. Mehtab, M.F.A. Santos, T. Santos-Silva, Inorg. Chim. Acta 420 (2014) 60–68.
[20] T. Jakusch, D. Hollender, É. Enyedy, C.S. Gonzáles, M. Montes-Bayón, A. Sanz-Medel, J.C. Pessoa, I. Tomaz, T. Kiss, Dalton Trans. (2009) 2428–2437.
[21] T. Kiss, T. Jakusch, D. Hollender, Á. Dörnyei, É.A. Enyedy, J.C. Pessoa, H. Sakurai, A. Sanz-Medel, Coord. Chem. Rev. 252 (2008) 1153–1162.
[22] T. Jakusch, A. Dean, T. Oncsik, A.C. Benyei, V. Di Marco, T. Kiss, Dalton Trans. (2010) 212–220.
[23] D.M. Dias, J.P.G.L.M. Rodrigues, N.S. Domingues, A.M.J.J. Bonvin, M.M.C.A. Castro, Eur. J. Inorg. Chem. (2013) 4619–4627.
[24] R.R. Gagne, C.A. Koval, G.C. Lisensky, Inorg. Chem. 19 (1980) 2854–2855.
[25] G.M. Sheldrick, Acta Cryst A64 (2008) 112–122.
[26] Klaus Brandenburg, DIAMOND 3.1a. 1997–2005, Version 1.1a. Crystal Impact GbR, Bonn, Germany.
[27] A.W. Addison, T.N. Rao, J. Reedijk, J. van Rijn, G.C. Verschoor, J. Chem. Soc. Dalton Trans. (7) (1984) 1349–1356.
[28] O.A. Chaves, C.S.H. Jesus, P.F. Cruz, C.M.R. Sant'Anna, R.M.M. Brito, C. Serpa, Spectrochim. Acta A Mol. Biomol. Spectrosc. 169 (2016) 175–181.
[29] A.P.O. Amorim, M.C.C. de Oliveira, T.A. Amorim, A. Echevarria, Antioxidants 2 (2013) 90–99.
[30] G.L. Ellman, K.D. Courtney, V. Andres, R.M. Feather-Stone, Biochem.Pharmacol. 7 (1961) 88–90.
[31] W.T. Ismaya, H.J. Rozeboom, A. Weijn, J.J. Mes, F. Fusetti, H.J. Wichers, B.W. Dijkstra, Biochemistry 50 (2011) 5477–5486.
[32] M. Harel, I. Schalk, L. Ehret-Sabatier, F. Bouet, M. Goeldner, C. Hirth, P.H. Axelsen, I. Silman, J.L. Sussman, Proc. Natl. Acad. Sci. 90 (1993) 9031–9035.
[33] D. Sousa-Pereira, O.A. Chaves, C.M. dos Reis, M.C.C. de Oliveira, C.M.R. Sant'Anna, J.C. Netto-Ferreira, A. Echevarria, Bioorg. Chem. 81 (2018) 79–87.
[34] S. Nica, M. Rudolph, I. Lippold, A. Buchholz, H. Görls, W. Plass, J. Inorg. Biochem. 147 (2015) 193–203.
[35] H. Hosseini-Monfared, A. Farrokhi, S. Alavi, P. Mayer, Transit. Met. Chem. 38 (2013) 267–273.
[36] F. Wu, C.-J. Wang, H. Lin, A.-Q. Jia, Q.-F. Zhang, Inorg. Chim. Acta 471 (2018) 718–723.
[37] I. Sheikhshoaie, S.Y. Ebrahimipour, N. Lotfi, J.T. Mague, M. Khaleghi, Inorg. Chim. Acta 442 (2016) 151–157.
[38] M. Asadi, Z. Asadi, N. Savaripoor, M. Dusek, V. Eigner, M.R. Shorkaei, M. Sedaghat, Spectrochim. Acta A Mol. Biomol. Spectrosc. 136 (2015) 625–640.
[39] D.F. Back, G.M. de Oliveira, D. Roman, M.A. Ballin, R. Kober, P.C. Piquini, Inorg. Chim. Acta 412 (2014) 6–14.
[40] H. Hosseini-Monfared, R. Bikas, P. Mahboubi-Anarjan, A.J. Blake, V. Lippolis, N.B. Arslan, C. Kazak, Polyhedron 69 (2014) 90–102.
[41] A.C. González-Baró, V. Ferraresi-Curotto, R. Pis-Diez, B.S.P. Costa, J.A.L.C. Resende, F.C.S. de Paula, E.C. Pereira-Maia, N.A. Rey, Polyhedron 135 (2017) 303–310.
[42] H. Hosseini-Monfared, S. Kheirabadi, N.A. Lalami, P. Mayer, Polyhedron 30 (2011) 1375–1384.
[43] W. Plass, H.-P. Yozgatli, J. Inorg. Gen. Chem. 629 (2003) 65–70.
[44] X. Liu, X. Ying, Y. Li, H. Yang, W. Hao, M. Yu, Spectrochim. Acta A Mol. Biomol. Spectrosc. 203 (2018) 383–396.
[45] S. Naveenraj, S. Anandan, J. Photochem. Photobiol. C 14 (2013) 53–71.
[46] M. Montalti, A. Credi, L. Prodi, M.T. Gandolfi, Handbook of Photochemistry, 3rd ed., CRC Press, Taylor & Francis, 2006.
[47] W. Plass, A. Pohlmann, H.-P. Yozgatli, J. Inorg. Biochem. 80 (2000) 181–183.
[48] A. Pohlmann, S. Nica, T.K.K. Luong, W. Plass, Inorg. Chem. Commun. 8 (2005) 289–292.
[49] S. Rudra, S. Dasmandal, C. Patra, A. Mahapatra, J. Mol. Struct. 1167 (2018) 107–117.
[50] M.B. Bolattin, S.T. Nandibewoor, S.D. Joshi, S.R. Dixit, S.A. Chimatadar, Ind. Eng. Chem. Res. 55 (2016) 5454–5464.
[51] K. Gałęcki, K. Hunter, G. Daňková, E. Rivera, L.W. Tung, K.M. Sherry, J. Lumin. 177 (2016) 235–241.
[52] O.A. Chaves, C.H.C.S. de Oliveira, R.C. Ferreira, R.P. Pereira, J.L.R. de Melos, C.E. Rodrigues-Santos, A. Echevarria, D. Cesarin-Sobrinho, J. Fluor. Chem. 199 (2017) 103–112.
[53] P. Temboot, F. Usman, Z. Ul-Haq, R. Khalil, T. Srichana, Spectrochim. Acta A Mol. Biomol. Spectrosc. 205 (2018) 442–456.
[54] C.G. Chilom, M. Bacalum, M.M. Stanescu, M. Florescu, Spectrochim. Acta A Mol. Biomol. Spectrosc. 204 (2018) 648–656.
[55] O.A. Chaves, R.C. Ferreira, L.S. da Silva, B.C.E. de Souza, D. Cesarin-Sobrinho, J.C. Netto-Ferreira, C.M.R. Sant'Anna, A.B.B. Ferreira, J. Braz. Chem. Soc. 29 (2018), pp. 1551–1562.
[56] P.D. Ross, S. Subramanian, Biochemistry 20 (1981) 3096–3102.
[57] X. Du, Y. Li, Y.-L. Xia, S.-M. Ai, J. Liang, P. Sang, X.-L. Ji, S.-Q. Liu, Int. J. Mol. Sci. 17 (2016) 144–177.
[58] N. Gan, Q. Sun, P. Tang, D. Wu, T. Xie, Y. Zhang, H. Li, Spectrochim. Acta A Mol. Biomol. Spectrosc. 206 (2019) 126–134.
[59] O.A. Chaves, L.S. de Barros, M.C.C. de Oliveira, C.M.R. Sant'Anna, A.B.B. Ferreira, F.A. da Silva, D. Cesarin-Sobrinho, J.C. Netto-Ferreira, J. Fluor. Chem. 199 (2017) 30–38.
[60] O.A. Chaves, C.S.H. Jesus, E.S. Henriques, R.M.M. Brito, C. Serpa, Photochem. Photobiol. Sci. 15 (2016) 1524–1535.
[61] A. Hosainzadeh, M. Gharanfoli, M.R. Saberi, J.K. Chamani, J. Biomol. Struct. Dyn. 29 (2012) 1013–1050.
[62] O.A. Chaves, D. Cesarin-Sobrinho, C.M.R. Sant'Anna, M.G. de Carvalho, L.R. Suzart, F.E.A. Catunda-Junior, J.C. Netto-Ferreira, A.B.B. Ferreira, J. Photochem. Photobiol. A 336 (2017) 32–41.
[63] G. Sudlow, D.J. Birkett, D.N. Wade, Mol. Pharmacol. 12 (1976) 1052–1061.